An official publication of the International Society for Energy, Environment and Sustainability (ISEES)

Journal of Energy and Environmental Sustainability

Journal homepage : www.jees.in

CFD Simulations of Complete Circulating Dual Fluidized Bed Systems for Chemical Looping Combustion

Subhodeep Banerjee, Xiao Zhang, Ramesh K. Agarwal*

Washington University in St. Louis, 1 Brookings Dr., St. Louis, MO 63130, USA

ARTICLE INFO

Received : 12 September 2015
Revised : 28 November 2015
Accepted : 29 November 2015

Keywords:
Chemical Looping, Dual Fluidized Bed Reactors, Multi-phase Flow, Granular Flow Eulerian Simulation, Discrete Element Method

ABSTRACT

Chemical-looping combustion (CLC) is a next generation combustion technology that shows great promise in addressing the need for high-efficiency low-cost carbon capture from fossil fueled power plants. Although there have been a multitude of experimental studies on CLC in recent years, the number of CFD simulations in the literature has been more limited. In this paper, simulation of a CLC reactor is developed using the Eulerian approach in the commercial CFD solver ANSYS Fluent based on a laboratory-scale experiment with a dual fluidized bed CLC reactor to model the chemical reactions in the system. The solid phase consists of a Fe-based oxygen carrier while the gaseous fuel used is syngas. Later, the detailed hydrodynamics in a CLC system designed for solid coal fuel are studied based on a cold flow experimental setup at National Energy Technology Laboratory using the Lagrangian particle-tracking approach. To the authors' knowledge, this work is among the very few CFD simulations of a complete circulating dual fluidized bed system for CLC in three-dimension. It highlights the importance of 3-D simulation of CLC systems and the need for more accurate empirical reaction rate data for future CLC simulations.

1. Introduction

The relationship between the global surface temperature of the Earth and the concentration of CO2 was discovered by Arrhenius (1896). The concentration of CO2 in the atmosphere has risen from a value of 280 ppm in pre-industrial times to around 370 ppm today. This increase is due to the carbon emissions from fossil fueled power plants and other anthropogenic sources. Since fossil fuels remain the world's main energy source, there is an imminent need for high-efficiency carbon capture technologies to avoid the unequivocal warming of the global climate system (IPCC, 2007). One technology that has shown great promise in recent years for high-efficiency low-cost carbon capture is chemical-looping combustion (CLC).

The CLC process typically utilizes dual fluidized bed reactors-an air reactor and a fuel reactor-and a metal oxide oxygen carrier that circulates between the two reactors, as illustrated in Figure 1(a). Another setup for CLC that has been documented in the literature employs a single vessel with a packed bed of oxygen carrier that is alternatingly used as an air and fuel reactor via a high temperature gas switching system, shown in Figure 1(b). The main advantage of CLC is that the combustion of fuel in the fuel reactor takes place in the absence of air using oxygen provided by the oxygen carrier. Thus, the flue stream from the fuel reactor is not contaminated or diluted by gases such as nitrogen. This provides a high-purity CO2 stream available for capture at the fuel reactor outlet without the need for an expensive gas separation process. The reduced oxygen carrier from the fuel reactor is pneumatically transported to the air reactor where it is re-oxidized by oxygen from air and circulated back to the fuel reactor to complete the loop.

The only energy cost of separation associated with CLC is the cost of solid recirculation; research has shown that this is only about 0.3% of the total energy released by the CLC process (Lyngfelt et al., 2001). This is considerably lower than the benchmark for pre-combustion technologies for carbon capture such as oxy-fuel combustion where the oxygen separation process can consume about 15% of the total energy. Therefore, CLC holds promise as the next-generation combustion technology due to its potential to allow CO2 capture with little effect on the efficiency of the power plant. Several studies on the energy and exergy of CLC systems in the literature suggest that power efficiencies greater than 50% can be achieved along with nearly complete CO2 capture (Ishida et al., 1987, 1996; Wolf et al., 2001; Marion, 2006; Andrus et al., 2008).

The oxygen carrier used in CLC directly affects the performance of the CLC system. Since iron is among the cheapest and most abundant metals available on Earth, Fe-based metal oxides such as hematite (Fe2O3) are commonly used as the oxygen carrier for CLC. However, past experience with CFD simulations employing the discrete element method has shown that the mass of a fluidized bed of pure Fe2O3 particles, given its density of 5,240 kg/m^3, is too large and impedes successful fluidization (Banerjee and Agarwal, 2015a). There are also issues with particle agglomeration at high temperatures. The use of an oxygen carrier based on Fe combined with an inert support material has been proposed to circumvent the drawbacks of the pure Fe2O3 oxygen carrier (Hossain and de Lasa, 2008). The analysis of several iron oxide particles has

* *Corresponding Author: Email: rka@wustl.edu; Phone: +1-314-935-6091*

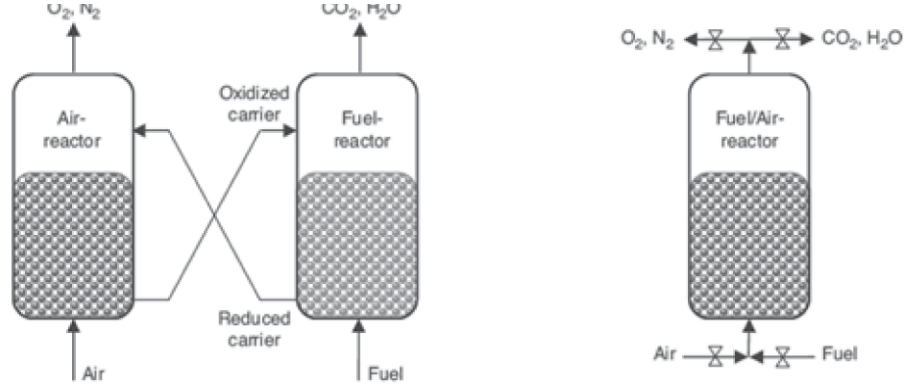

Figure 1: Schematic representation of a chemical-looping combustion system with (a) interconnected fluidized beds, and (b) packed bed with alternating flow (Kruggel-Emden et al., 2011)

shown that an oxygen carrier consisting of 60% Fe2O3 by mass and 40% Al2O3 provides excellent reactivity for use in CLC and its hardness and resistance to agglomeration is ideal for fluidized bed operation (Johansson, 2007). The Al2O3 is inert and acts as a porous support providing a higher surface area for reaction.

Setting up and executing a laboratory experiment can be an expensive and laborious process. On the other hand, CFD provides an efficient means to analyze the performance of a CLC system and characterize the fluid mechanics and chemical kinetics in the system. Initial CFD studies in the field demonstrated the capability of computational methods to model a CLC system and were not based on any particular experiment (Jung and Gamwo, 2008; Deng et al., 2008). Later, the work of Mahalatkar et al. (2011a, 2011b) based on a single reactor setup similar to Figure 1(b) showed that CFD simulation is able to match the reaction mechanics inside a CLC fuel reactor with reasonable accuracy. However, the single reactor setup "cannot be operated with solid fuels and the design and operation of the hot gas switching system is problematic" (Kruggel-Emden et al., 2011). It is desirable to use solid coal for CLC operation due to its likelihood to remain the dominant fossil fuel in the near future, necessitating the use of the dual fluidized bed setup shown in Figure 1(a). The single reactor simulations do not provide any information about the circulation of oxygen carrier inside a dual fluidized bed setup. Therefore, it is important to establish a credible CFD simulation based on a dual fluidized bed setup for CLC.

In the present study, the laboratory experiment of Abad et al. (2007) is used as a basis to perform a detailed CFD simulation of a CLC system. The Eulerian or continuum approach is used for modeling the solid phase. The fluidization behavior in both air and fuel reactor beds and the circulation of the oxygen carrier between the beds is investigated and compared with the experiment. Chemical reactions in the fuel reactor are also considered and the CFD data is validated against the outlet concentrations of various flue gases. Later, the cold flow behavior of the full CLC system at National Energy Technology Laboratory (NETL) is modeled in three dimensions employing the Lagrangian discrete element method (DEM) to follow up on the CFD simulation conducted for this case previously by Parker (2012). The tracking of individual solid particles in time and their interactions with each other as well as with the ambient fluid provide an accurate and realistic representation of the multiphase flow field. These simulations in this work are among the very few present in the current literature of a complete circulating dual fluidized bed setup.

2. Eulerian Simulation of the Experimental CLC Reactor of Abad et al (2007)

In this section, the laboratory scale experiment of Abad et al. (2007) is used as a basis to perform a detailed CFD simulation of a CLC system using the Eulerian multi-fluid approach. It is one of the first CFD models of a complete circulating dual fluidized bed setup. The fluidization behavior in both air and fuel reactor beds and the circulation of the oxygen carrier between the beds is investigated and compared with the experiment. Chemical reactions in the fuel reactor are also considered and the CFD data is validated against the outlet concentrations of various flue gases.

2.1 Description of Experimental Setup

The experiment uses the two-compartment fluidized bed design proposed by Chong et al. (1986) and further investigated by Yang et al. (2003). The experimental reactor setup is illustrated in Figure 2 (a). Dimensions and additional details can be found in the work of Abad et al. (2007). The experiment used a Fe-based oxygen carrier consisting of 60% Fe2O3 by mass and 40% Al2O3. The particular batch of oxygen carrier used by Abad et al. (2007) was sintered at 1100ºC and is designated as F6A1100. The gaseous fuels used in the experiment are natural gas, consisting of primarily CH4 and syngas consisting of a mixture of 50% CO and 50% H2. The oxygen carrier particles in the air reactor are oxidized in the presence of air; the fluidizing velocity is greater than the terminal velocity of the particles and carries the particles upwards. The flow then undergoes a sudden expansion in the particle separator at the top of the reactor, which causes the particles to fall back down into the down-comer and enter the fuel reactor.

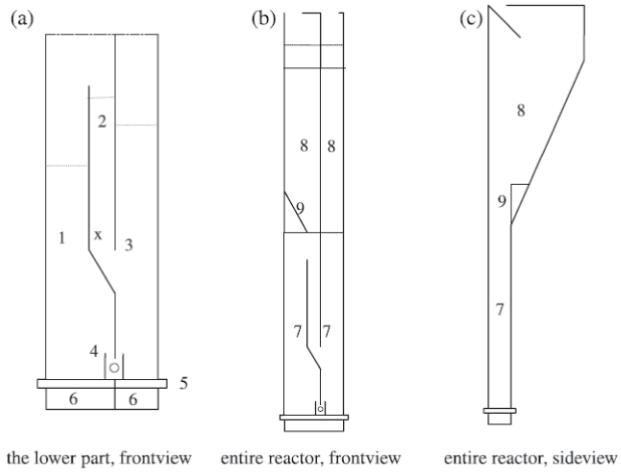

Figure 2 (a): Sketch of experimental reactor: (1) air reactor, (2) down-comer, (3) fuel reactor, (4) slot, (5) gas distributor plate, (6) wind box, (7) reactor part, (8) particle separator, (9) leaning wall. The symbols (x) and (o) indicate fluidization in the down-comer and slot.

The fluidizing velocity in the fuel reactor is below the terminal velocity of the particles, therefore a bubbling bed behavior is exhibited. Therefore, the particles do not reach the particle separator in the fuel reactor. The pressure in the fuel reactor is controlled via a water trap connected to the flue stream of the reactor to ensure minimal gas leakage between the fuel reactor and the air reactor through the down-comer and slot. The flue streams from both reactors are led to a gas analyzer (Rosemount, model NGA-2000) where the concentrations of various gases are measured.

2.2 Numerical Solution Procedure

The modeling work in this paper is performed using the commercial CFD simulation package ANSYS Fluent, release version 14.5 (ANSYS, 2012a, 2012b). Since the flow inside the CD-CLC fuel reactor is chemically active with heat transfer, all the equations of fluid dynamics - the continuity equation, the Navier-Stokes momentum equations, and the energy equation - are considered to compute the flow field. The solid phase is approximated as an Eulerian fluid phase whereby particle variables such as mass, velocity, temperature, etc. are averaged over a region that is large compared to the particle size. Thus, the Eulerian approach only accounts for the bulk behavior of the solids. Constitutive equations for the solid phase pressure and viscosity are required to model the interactions between the solid and gas phases. These are provided by the kinetic theory of granular flow, which is an extension of the classical kinetic gas theory that includes inelastic inter-particle interactions (Patil et al., 2004a, 2004b). The Eulerian framework for modeling a multiphase flow involving a granular solid and a gas has been in use for a few decades and has proven reliable in capturing the experimental behavior.

2.1.1. Eulerian Two-Fluid Model Equations

The standard set of fluid dynamics equations that are used in the commercial CFD software ANSYS Fluent are well-documented in the literature. For multiphase simulations using the Eulerian approach, the standard equations of fluid motion are slightly modified to account for the presence of additional phases by including the porosity ? defined as the volume fraction of the respective phase in the computational cell where the equations are applied (ANSYS, 2012b). The continuity equation for phase q is given as

$$\frac{\partial}{\partial t}\left(\alpha_q \rho_q\right) + \nabla \cdot \left(\alpha_q \rho_q \boldsymbol{u}_q\right) = \sum\left(\dot{m}_{pq} - \dot{m}_{qp}\right) \tag{1}$$

where m ?_pq is the mass transfer rate from the pth phase to the qth phase. Each phase (gas or solid) consists of a number of species. A transport equation is solved for each species,

$$\frac{\partial}{\partial t}\left(\alpha_q \rho_q Y_{iq}\right) + \nabla \cdot \left(\alpha_q \rho_q \boldsymbol{u}_q Y_{iq}\right) = \sum\left(\dot{m}_{ij}^{qp} - \dot{m}_{ji}^{pq}\right) \tag{2}$$

where Y_iq is the mass fraction of the species i in the qth phase and m ?_ij^qp is the mass transfer rate from the jth species of the pth phase to the ith species in the qth phase. In the present study, one gas phase and one solid phase is considered, corresponding to the fuel-gas mixture and the oxygen carrier respectively.

The momentum equation for the gas phase is given as

$$\frac{\partial}{\partial t}\left(\alpha_g \rho_g \boldsymbol{u}_g\right) + \nabla \cdot \left(\alpha_g \rho_g \boldsymbol{u}_g \boldsymbol{u}_g\right) = -\alpha_g \nabla p + \nabla \cdot \bar{\bar{\tau}}_g + \alpha_g \rho_g \boldsymbol{g} + \sum\left(\boldsymbol{R}_{sg} + \dot{m}_{sg}\boldsymbol{u}_{sg} - \dot{m}_{gs}\boldsymbol{u}_{gs}\right) \tag{3}$$

where the terms in the summation are source terms added to the standard form of the Navier-Stokes momentum equations to account for the momentum transfer between the solid phase and the gas phase. Specifically, $R_{sg}=b_{sg}(u_s-u_g)$ is the momentum transfer due to interphase drag and the other terms are due to the transfer of mass. The momentum equation for the solid phase follows from the momentum equation for the gas phase with the source term for interphase drag being equal but opposite.

$$\frac{\partial}{\partial t}\left(\alpha_s \rho_s \boldsymbol{u}_s\right) + \nabla \cdot \left(\alpha_s \rho_s \boldsymbol{u}_s \boldsymbol{u}_s\right) = -\alpha_s \nabla p + \nabla \cdot \bar{\bar{\tau}}_s + \alpha_s \rho_s \boldsymbol{g} + \sum\left(\boldsymbol{R}_{rs} + \dot{m}_{rs}\boldsymbol{u}_{rs} - \dot{m}_{sr}\boldsymbol{u}_{sr}\right) \tag{4}$$

For the flow conditions in a fuel reactor, the gas can be considered as an incompressible fluid. The fluid stress tensor is simply the Cauchy stress tensor with zero bulk viscosity.

$$\bar{\bar{\tau}}_g = \alpha_g \mu_g \left(\nabla \boldsymbol{u}_g + \nabla \boldsymbol{u}_g^T\right) \tag{5}$$

On the other hand, the granular solid stress tensor considers all terms in the Cauchy stress tensor,

$$\bar{\bar{\tau}}_s = -p_s \bar{\bar{I}} + \alpha_s \mu_s (\nabla \boldsymbol{u}_s + \nabla \boldsymbol{u}_s^T) + \alpha_s \lambda_s (\nabla \cdot \boldsymbol{u}_s)\bar{\bar{I}} \tag{6}$$

where p_s is the solids pressure, μ_s is the granular viscosity, and λ_s is the granular bulk viscosity. The definition of these terms and the interphase exchange coefficient β_{sg} provide the basis for the Eulerian approach for multiphase flow simulation. The solids pressure and granular bulk viscosity used in the present work are according to Lun et al. (1984); the granular viscosity is according to Gidaspow (1992).

The experiment of Abad et al. (2007) utilizes a riser and a bubbling bed for the air reactor and the fuel reactor respectively whereas the down-comer resembles a packed bed. Therefore, the simulation is expected to include a range of solid loadings from dilute to densely packed. The Gidaspow model is well-suited for this work because it accounts for the differences in the solid-gas interaction behavior in dilute and dense regions by switching between the drag prediction of the Ergun equation (Ergun, 1952) and the drag model of Wen and Yu (1966) based on the solids fraction αs. For αs>0.8, the Gidaspow model for the exchange coefficient β_{sg} gives

$$\beta_{sg} = \frac{3}{4} C_D \frac{\alpha_s \alpha_g \rho_g |\boldsymbol{u}_s - \boldsymbol{u}_g|}{d_s} \alpha_g^{-2.65}; C_D = \frac{24}{\alpha_g \mathrm{Re}_s}\left[1 + 0.15\left(\alpha_g \mathrm{Re}_s\right)^{0.687}\right] \tag{7}$$

Conversely, for αs ≤ 0.8,

$$\beta_{sg} = 150 \frac{\alpha_s (1-\alpha_g)\mu_g}{\alpha_g d_s^2} + 1.75 \frac{\rho_g \alpha_s |\boldsymbol{u}_s - \boldsymbol{u}_g|}{d_s} \tag{8}$$

where d_s is the particle diameter and Re_s is the Reynolds number based on d_s.

Finally, the energy equation for phase q is expressed in terms of the enthalpy as

$$\frac{\partial}{\partial t}\left(\alpha_q \rho_q h_q\right) + \nabla \cdot \left(\alpha_q \boldsymbol{u}_q h_q\right) = \alpha_q \frac{\partial p}{\partial t} + \nabla \cdot \left(\bar{\bar{\tau}}_q \cdot \boldsymbol{u}_q\right) - \nabla \cdot \boldsymbol{q}_q + S_q + \sum \boldsymbol{Q}_{pq} \tag{9}$$

where h_q and q_q are the specific enthalpy and heat flux of phase q respectively. As with the continuity and momentum equations, source terms are implemented to account for the transfer of enthalpy between phases. In particular, S_q is the enthalpy source due to chemical reaction and Q_{pq} is the heat transfer from the pth phase to the qth phase. The interphase heat transfer in the current simulation is modeled based on Gunn (1978).

2.2.2 Chemical Reaction Scheme and Rates

The oxygen carrier used in the numerical simulation is F6A1100, consisting of 60% Fe_2O_3 and 40% inert Al_2O_3 by mass, following the experiment of Abad et al. (2007). Of the two gaseous fuels used in the experiment, only syngas has been considered in the current work because the chemical kinetics for the reaction of Fe_2O_3 with the non-methane components of natural gas is not available. The metal oxide reduction reactions that are used in the simulation are

$$3\,Fe_2O_3 + CO \rightarrow 2\,Fe_3O_4 + CO_2 \tag{10}$$

$$3\,Fe_2O_3 + H_2 \rightarrow 2\,Fe_3O_4 + H_2O \tag{11}$$

Exact reaction rates for the reduction of F6A1100 with CO and H_2 are not available in the literature; the reaction rates are assumed to be the same as the reduction rates for hematite (pure Fe_2O_3) with CO and H_2 obtained from the experiment of Mattisson et al. (2005) and further developed by Mahalatkar et al. (2011b) for the simulation of chemical reactions in a single fuel reactor with solid fuel. Based on these papers, the reaction rates m ? (in kg/s per cell volume or kg/(m³-s)) of the fuel gases with Fe_2O_3 are given by

$$\dot{m}_{\mathrm{H_2}} = \frac{k_{\mathrm{H_2}} R_o}{2MW_{\mathrm{O_2}}} \rho_{avg} \alpha_s \left(Y_{\mathrm{Fe_2O_3}} + Y_{\mathrm{Fe_3O_4}} \frac{\nu_{\mathrm{Fe_2O_3}} MW_{\mathrm{Fe_2O_3}}}{\nu_{\mathrm{Fe_3O_4}} MW_{\mathrm{Fe_3O_4}}}\right)(1-X)^{2/3} MW_{\mathrm{H_2}} \tag{12}$$

and

$$\dot{m}_{\mathrm{CO}} = \frac{k_{\mathrm{CO}} R_o}{2MW_{\mathrm{O_2}}} \rho_{avg} \alpha_s \left(Y_{\mathrm{Fe_2O_3}} + Y_{\mathrm{Fe_3O_4}} \frac{\nu_{\mathrm{Fe_2O_3}} MW_{\mathrm{Fe_2O_3}}}{\nu_{\mathrm{Fe_3O_4}} MW_{\mathrm{Fe_3O_4}}}\right)(1-X)^{2/3} MW_{\mathrm{CO}} \tag{13}$$

where k is the nominal reaction rate based on the Arrhenius rate, R_o is the oxygen carrying capacity, MW is the molecular weight (in kg/kmol),

Y is the mass fraction, ? is the stoichiometric coefficient, and X is the conversion fraction based on the fully reduced state; in each case, the subscript identifies the species under consideration. More details of the reaction rate derivation can be found in the work of Mahalatkar et al. (2011b). The reaction rates identified in Eq. (12) and Eq. (13) are implemented into the numerical simulation through separate user-defined functions.

2.3. Three-dimensional Simulation of Abad et al. Experiment

The results of the 2-D simulation of the experiment of Abad et al. (2007) were discussed in previous work (Banerjee and Agarwal, 2015b). Although the 2-D model successfully captured the salient features of the fluidization behavior in the dual fluidized bed system, it was unable to produce the expected concentrations of CO_2 and H_2O in the fuel reactor because of the inadequacy of the 2-D simulation in modeling the gaseous diffusion, which is an inherently 3-D process. Therefore, a 3-D simulation of Abad et al.'s experiment is considered in this work to obtain a closer fit for the chemical reactions between the simulation and experiment. The 3-D computational domain is an exact representation of the geometry of Abad et al. (2007) shown in Figure 2 (a). A structured mesh is used with a relatively fine grid in the lower part of the reactor and a coarser grid in the upper regions. The mesh used for the 3-D simulations is shown in Figure 2(b).

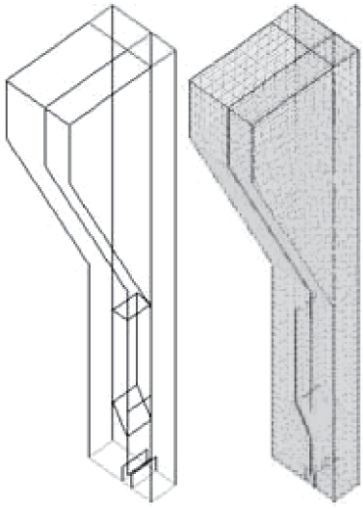

Figure 2(b): Computational domain (L) and grid (R) for 3-D CFD simulation

The oxygen carrier used in the experiment has an apparent density of 2,150 kg/m³ and porosity of 0.56 with a diameter of 90-212 ?m; the average value of 150 ?m is used in the simulation. The initial solids loading in the bed is about 300 g, of which 110 g is in the fuel reactor, in line with the experiment. The reactors are set to atmospheric pressure and the gage pressures at the outlets are set at zero. The pressure differential between the reactors, controlled by a water trap in the experiment to minimize leakage, was not implemented in the simulation because the data was not available. It is expected that the pressure differential is a secondary mechanism and the dense solid packing in the down-comer and slot will be sufficient to keep the leakage to a minimal. Lastly, the temperature for the simulation was set at 1123 K, in line with the reference condition specified from the experiment. The numerical parameters used in the CFD simulation are summarized in Table 1. It should be noted that the secondary phase mass fraction has been set to zero at both fuel and air reactor inlets, i.e., no new oxygen carrier is added.

The experiment of Abad et al. (2007) was operated for 60 hours without replacing the oxygen carrier or adding new material. However, the complete reactor simulation of 60 hours is beyond the scope of CFD at this time. Instead, the initial batch processing results of Abad et al. (2007) are used to validate the CFD simulation in the present work. For these batch operations, the initial oxygen carrier mass in the fuel reactor is sufficient for reacting with all the incoming fuel, so the fuel conversion is not affected by the re-oxidation in the air reactor. The CFD simulation is thus considerably simplified by setting the fluidization gas in the air reactor to an inert gas (in this case, nitrogen).

Table 1: Modeling parameters for 3-D CFD simulation of the Abad et al. experiment

Primary phase	Fuel-gas mixture
Secondary phase	Oxygen carrier (F6AL1100)
Average particle diameter	150 ìm
Average particle density	2150 kg/m³
Initial bed mass	~180 g
Fluidizing gas composition in fuel reactor	50% CO, 50% H_2
Fluidizing gas composition in air reactor	100% N_2
Inlet boundary condition in fuel reactor	Velocity inlet with velocity 0.1 m/s
Inlet boundary condition in air reactor	Velocity inlet with velocity 0.5 m/s
Outlet boundary condition in fuel reactor	Pressure outlet at atmospheric pressure
Outlet boundary condition in air reactor	Pressure outlet at atmospheric pressure
Operating temperature	1123 K
Solids pressure	Lun et al. (1984)
Granular bulk viscosity	Lun et al. (1984)
Granular viscosity	Gidaspow (1992)
Drag law	Gidaspow (1992)
Heat transfer coefficient	Gunn (1978)
Numerical scheme	Phase-coupled SIMPLE
Time step size	0.0005 s
Iterations per time step	20

The 3-D simulation was run on a Dell workstation with a quad-core Intel Xeon CPU. 30 seconds of simulation completed in approximately 96 hours. The contours of the mass fraction of CO_2 for the 3-D simulation are shown in Figure 2(c). In comparison to the 2-D simulation results (Banerjee and Agarwal, 2015b), there is greater diffusion in the 3-D case as expected. The local mass fraction of CO_2 at the base of the bed, where the injected CO first comes into contact with the Fe_2O_3 and begins to react is around 15%. Owing to the increased diffusion in 3-D, the CO_2 spreads through the fuel reactor more homogeneously as it travels towards the fuel reactor outlet; the vortex patterns seen in the 2-D case are absent. The contours of the mass fraction of H_2O display the same characteristics. The quantitative effects of this can be observed from the plot of the mass fractions of CO_2 and H_2O at the fuel reactor outlet given in Figure 3. The mass fractions of both CO_2 and H_2O are initially lower than in the 2-D case. This is because these gases now have to diffuse through the nitrogen present in the fuel reactor instead of displacing it and thus reach the outlet more slowly. The large fluctuations in the outlet mass fraction caused by pockets of reversed flow in the 2-D case are eliminated. Since reversed flow does not develop in the current simulation, the mass fractions keep increasing as the simulation progresses and more and more CO_2 and H_2O

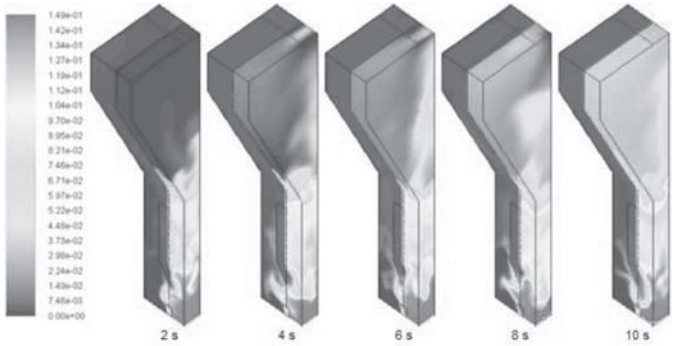

Figure 2(c): Contours of CO_2 mass fraction for the first ten seconds of 3-D simulation showing the increased diffusion and absence of the vortex pattern compared to the 2-D case

are produced. By 20 seconds, the mass fractions of both CO_2 and H_2O have exceeded their stagnation values from the 2-D simulation (shown by dotted lines in Figure 3). By 30 seconds, the mass fraction of H2O reaches the expected value from the batch experiments of Abad et al. (2007). However, it is noted that although the final outlet mass fraction of CO2 after 30 seconds is higher than the 2-D case, it does not reach the experimental value.

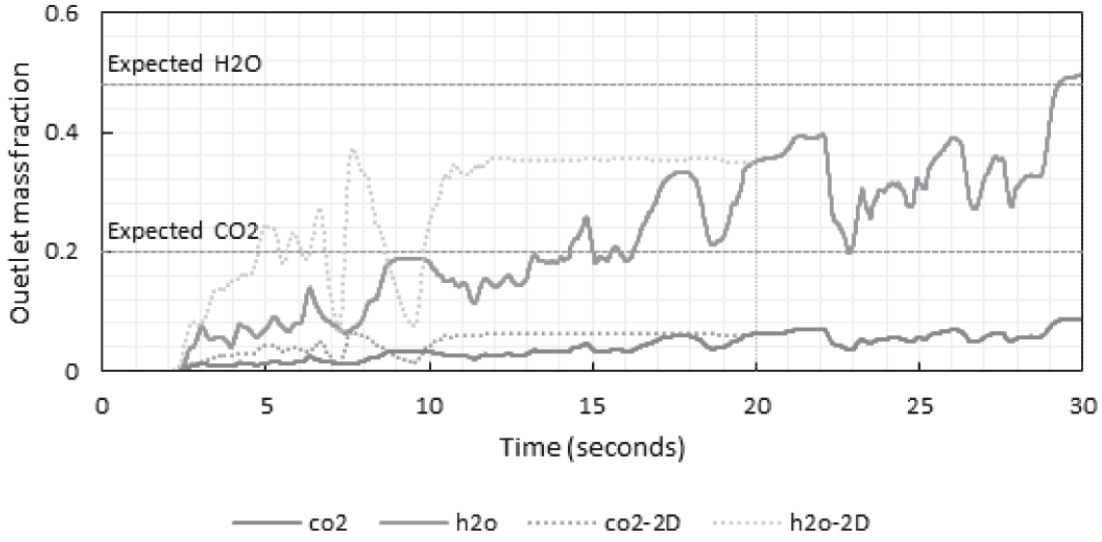

Figure 3: Mass fractions of CO_2 and H_2O at the fuel reactor outlet for the 3-D simulation

The 3-D simulation shows a significant improvement in the mass fraction measurements of the flue gases at the fuel reactor outlet. However, there is still some discrepancy in the mass fraction of CO_2, which may be due to various external factors. In Abad et al.'s experiment (2007), the gas streams from the reactors were pipelined to an electric cooler and then to the gas analyzer. The experiments of Taylor (1954) showed that significant apparent diffusion can occur in gases when they travel through pipes. Thus, it is reasonable to expect that the concentrations measured by Abad et al. (2007) in the gas analyzer may be different from the concentrations present right at the fuel reactor outlet. It should also be noted that the reaction rate kinetics used in the simulation were based on the experimental study of Mattisson et al. (2005) using hematite, whereas the oxygen carrier used in the experiment of Abad et al. (2007) was F6A1100. One of the reasons F6A1100 is preferred over Fe_2O_3 as the oxygen carrier for CLC operation is its improved reactivity, caused by an increase in apparent surface area due to the presence of the porous Al_2O_3 (Johansson, 2007). As such, it stands to reason that the experiment shows a higher concentration of the reaction products compared to the current simulation. Further research is required to determine more accurate empirical formulas for the reduction of F6A1100 specifically to improve the accuracy of the results of the CFD simulation.

3. Lagrangian Simulation of Complete CLC Reactor at NETL

The Eulerian two-fluid model can accurately capture the bulk behavior of the solid phase in the dual fluidized bed reactor for CLC using gaseous fuels. However, since coal is projected to remain one of the dominant fossil fuels in the near future, the concept of coal-direct chemical-looping combustion (CD-CLC) with in situ gasification has garnered significant interest in recent years. In a CD-CLC system, the oxygen carrier needs to be formed into particles with a relatively larger diameter compared to the pulverized coal for easier separation. The work of Gryczka et al. (2009) with the larger particles has suggested that accurate numerical representation of particle dynamics is not likely to be achieved using the multiphase granular solid phase approximation due to "the inadequacies of the continuum model." The inaccuracy arises from the non-physical closure terms used in the Eulerian model such as the frictional solids viscosity or the solids pressure based on the kinetic theory of granular flow. Thus, for a more detailed understanding of the hydrodynamics in a multiphase system inside a CLC reactor, the Lagrangian particle-based approach is employed to study the CD-CLC reactor system at National Energy Technology Laboratory, previously investigated by Parker (2012).

3.1. Description of Experimental Setup

The geometry of the CD-CLC system used at NETL comprises an air reactor, cyclone, loop-seal, and fuel reactor, as shown later in Figure 5(a). The entire geometry is approximately 12 ft. high. In the cold flow experiment, the oxygen carrier particles start from the bottom of the air reactor and move up along the riser and into the cyclone. In the cyclone, the particles are separated from the air stream and drop into the loop-seal due to the gravity. After passing through the slightly fluidized loop-seal, the particles move into the fuel reactor. The oxygen carrier particles leave the fuel reactor, pass through an L-valve and then return to the air reactor. Dimensions and additional descriptions of the various components of

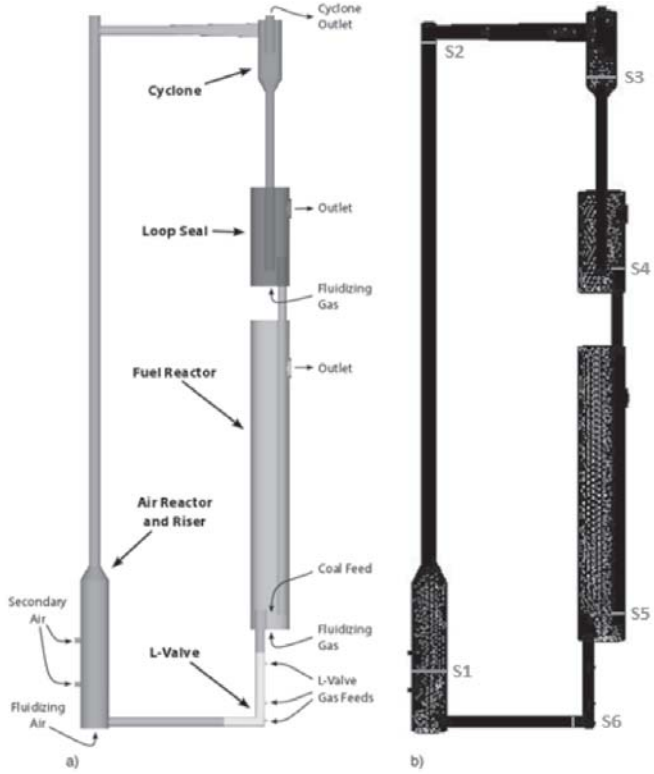

Figure 5(a): (a) Geometry of the coal-direct chemical-looping combustion system at NETL (Parker, 2012), and (b) computational mesh with static pressure measurement locations marked as “S”

the CD-CLC geometry of NETL can be found in the work of Parker (2012). The computational grid, also shown in Figure 6, is an exact representation of the geometry. The oxygen carrier particles in the cold flow experiment are primarily ilmenite ($FeTiO_3$) with some uncombined TiO_2 and Fe_2O_3 as well. The ilmenite particles had a size distribution of 13 μm to 320 μm. The particle size used in the numerical simulation corresponds to the median particle size of 150 ?m with the average density of ilmenite of 4,450 kg/m³.

3.2 Numerical Solution Procedure

The equations for mass and momentum conservation for the fluid phase are identical to those used in the Eulerian model given in Eqs. (1) and (3) with the exception that the source term in Eq. (3) for the solid-gas momentum exchange term, R_{sg}, is obtained from the average of the drag forces acting on all the discrete particles in a given computational cell. The shear stress term in the momentum equation is given in Eq. (5). Since the current simulation considers a cold flow with no species transport, the energy and species conservation equations are not applicable in this case.

3.2.1 Particle Equations

In the Lagrangian approach, each solid particle is tracked individually. The motion of each solid particle is obtained by summing the forces acting on the particle and applying Newton's second law of motion. The resulting force balance equation, which is integrated to obtain the motion of the solid particle, is given by

$$m_s \frac{\partial \boldsymbol{u}_s}{\partial t} = \sum \boldsymbol{F}_i = \boldsymbol{F}_{gra} + \boldsymbol{F}_{buo} + \boldsymbol{F}_{drag} + \boldsymbol{F}_{pre} + \boldsymbol{F}_{Saf} + \boldsymbol{F}_{Mag} + \boldsymbol{F}_{con} \tag{14}$$

In Equation (14), F_{gra} and F_{buo} are bulk forces due to gravity and buoyancy respectively. F_{drag}, F_{pre}, F_{Saf}, and F_{Mag} are hydrodynamic forces due to momentum transfer between the solid particles and the surrounding fluid, namely the drag force due to fluid viscosity, the pressure force due to pressure gradient, Saffman lift force due to inter-particle friction, and the Magnus force due to particle spin respectively. Owing to the large difference between the solid particle density and the fluid density, the pressure force can be dropped from Eq. (14) without loss of accuracy; the Magnus force can also be dropped because of negligible particle rotation.

F_{con} is the contact force on the particles due to collision with other particles or walls. In this paper, this contact force is computed using the soft-sphere model, which decouples its normal and tangential components (ANSYS, 2012b). The normal force on any particle involved in a collision is given by

$$\boldsymbol{F}_{con}^{n} = \left(k\delta + \gamma(\boldsymbol{u}_{12}\boldsymbol{e})\right)\boldsymbol{e} \tag{15}$$

where k is the spring constant of the particle, δ is the overlap between the particle pair involved in the collision as illustrated in Figure 4, γ is the damping coefficient, u_{12} is the relative velocity vector of the colliding pair, and *e* is the unit vector. For large values of k, the results of the soft-sphere model are interchangeable with those obtained using a hard-sphere model (Link, 1975). The tangential contact force is calculated based on the normal force as $F^{t}_{con} = \mu F^{n}_{con}$ where the coefficient of friction μ is given as a function of the relative tangential velocity v_r by

$$\mu(v_r) = \begin{cases} \mu_{stick} + (\mu_{stick} - \mu_{glide})(v_r/v_{glide} - 2)(v_r/v_{glide}) & \text{if } v_r < v_{glide} \\ \mu_{glide} & \text{if } v_r \geq v_{glide} \end{cases} \tag{16}$$

3.2.2. Solid-Gas Momentum Exchange

It is essential to evaluate the momentum exchange between the solid and fluid phase for multiphase flow modeling using the coupled CFD/DEM solver; this is done by considering the drag force. The transfer of momentum from the fluid to a solid particle as it moves through each cell in the computational domain is attributed to the drag force exerted on the particle by the fluid, and is modeled as

$$\boldsymbol{F}_{drag} = F_D(\boldsymbol{u}_f - \boldsymbol{u}_p) \tag{17}$$

where u_f is the fluid velocity, u_p is the particle velocity, and F_D is the net drag coefficient,

$$F_D = \frac{18\mu}{\rho_p d_p^2}\frac{C_D Re_p}{24} \tag{18}$$

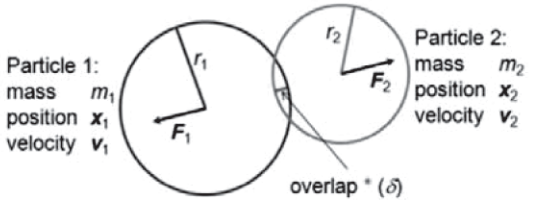

Figure 4: Schematic of particle collision model for DEM

where μ, p_p, and d_p are the viscosity of the gas and the density and diameter of the solid particle respectively. C_D and Re_p are the particle drag coefficient for a sphere and the relative Reynolds number based on the particle diameter respectively. Re_p is defined as

$$Re_p = \frac{\rho_f d_p |\boldsymbol{u}_f - \boldsymbol{u}_p|}{\mu} \tag{19}$$

The drag coefficient can be modeled using various empirical relations. The spherical or Stokes drag law is chosen in this work for its simplicity.

3.2.3. Parcel Concept

The computational cost of the DEM approach is driven by the number of collisions between particles; to track each individual particle in a CLC system using the DEM approach is extremely computationally demanding since the total number of particles increases drastically as the particle size becomes smaller. Therefore, the parcel methodology first proposed by Patankar and Joseph (2001) is employed in this work to overcome the high computational cost.

According to Patankar and Joseph (2001), one parcel can represent a group of particles with the same properties such as density and size. The mass used in collisions is that of the whole parcel rather than a single particle. By summing the mass and volume of each individual particle in the parcel, the total mass m_p and volume V_p of the parcel can be obtained. The radius of the parcel is then determined by the mass of the entire parcel and the particle density. For a given point in the fluid flow, the driving force of a parcel due to fluid forces is assumed to be the same as the sum of the fluid force acting on the group of particles it represents.

$$\boldsymbol{F}_{f,p} = \sum_{i=1}^{N_p} \boldsymbol{F}_{f,i} \tag{20}$$

where N_p is the number of particles in the parcel, and F_f is the net fluid force acting on a parcel p or particle i depending on the subscript. The acceleration due to inter-particle collision forces and particle-wall collisions forces are computed based on the mass properties of the parcel.

3.3. Cold Flow Simulation of NETL CD-CLC Reactor System

The boundary conditions for the cold flow simulation are obtained from Parker (2012) and are summarized in Table 2. Particles are injected into the air reactor, loop-seal, and air reactor and allowed to settle prior to the start of the simulation. A total of 717,879 particles in total are injected into the system-73,360 particles in the air reactor, 365,057 in the fuel reactor, and 279,462 in the loop-seal. After the particles are settled in each bed, the CFD/DEM model is run to simulate 360 ms of cold flow operation. The development of particle movement is shown in the Figure 5(b) at 10 ms intervals with the particles colored by velocity magnitude.

Table 2: Boundary conditions for cold flow simulation

Unit	Flow Boundaries		Flow rate (m/s)
	Boundary	Gas	
Air reactor	Fluidizing air	Air	20
Fuel reactor	Fluidizing gas	N_2	4
Loop-seal	Fluidizing gas	N_2	2
L-valve	Stripper (upper)	N_2	0.5
	Aeration (middle)	N_2	1
	Eductor (lower)	N_2	1
	Pressure Boundaries		
Unit	Boundary	Gas	Pressure (kPa)
Fuel reactor	Outlet	N_2	101.325
Loop-seal	Outlet	N_2	101.325
Cyclone	Outlet	Air	101.325

According to Figure 5(b), the particles in the air reactor reach the top of the riser at around 190 ms, and then move horizontally along the pipe towards the cyclone. The horizontal movement is driven by two secondary gas injections on the side of the air reactor. After another 40 ms, the particles enter the cyclone and start to drop down to the loop-seal. Due to an erroneously high gas velocity in the loop-seal and fuel reactor during the initial startup, the particles in these chambers are also shot up to the top. Once the gas injections are reduced to their correct values of 2 m/s and 4 m/s respectively at 210 ms, the particles settle down again. From this point on, it is expected that the particles in the loop-seal will drop into the fuel reactor and the L-valve, and finally be pushed back into the air reactor by the gas injection in the L-valve. 360 ms is not sufficient time to see the complete particle recirculation; however, the pressure contours in Figure 5(c) show the development of favorable pressure gradients for particle recirculation as simulation time increases.

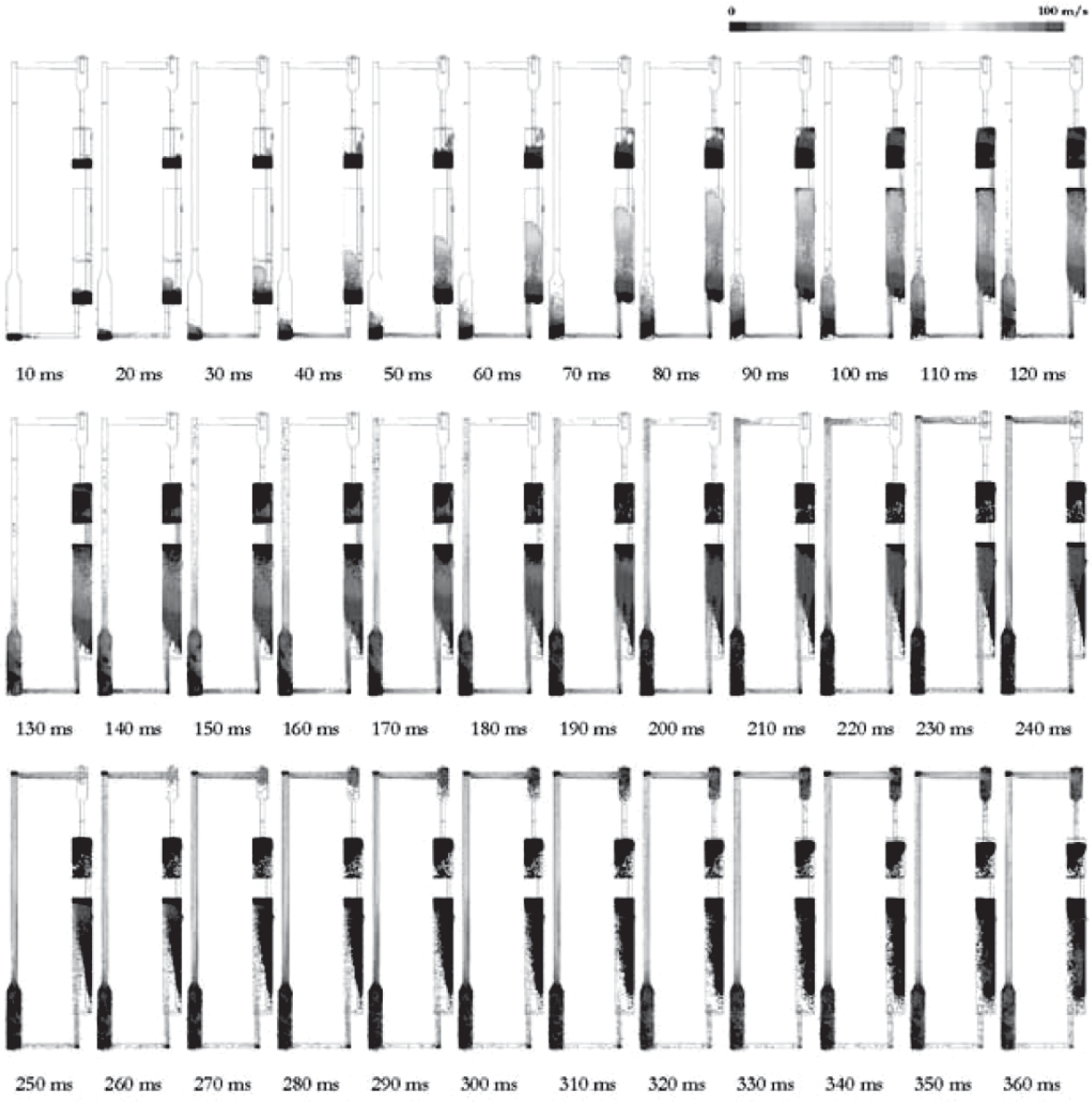

Figure 5(b): Particle tracks colored by velocity magnitude for the first 360 ms of cold flow simulation

The static pressure in the system is evaluated at the surfaces S1-S6 shown in Figure 5(a) to quantify the pressure gradients observed in Figure 5(c); the static pressures variation at 360 ms is presented in Figure 6. The arrows indicate the particle movement direction. It can be observed from Figure 6 that there is a consistent positive pressure differential between surface S1 (air reactor bed) through to S5 (fuel reactor bed), which confirms that particle continuous recirculation can occur between these surfaces. The pressure gradient between S5 and S1 via S6 (L-valve) is an adverse gradient. However, since the particle movement through the L-valve is driven by the gas injection into the L-valve, the adverse gradient does not affect the overall particle recirculation.

Conclusion

In this work, a 3-D CFD simulation for a complete circulating dual fluidized bed system was developed for chemical-looping combustion based on the 300 W laboratory-scale reported data. The oxygen carrier is modeled as an Eulerian fluid phase. The results of this study highlight the importance of capturing the 3D diffusion of gases in the reactor to ensure that accurate results are obtained for the chemical reactions. The 3-D model produced significantly improved results for the outlet concentrations of gases from the fuel reactor when compared to the experiment. The detailed particle hydrodynamics in a complete circulating CLC system for solid fuels was also investigated using the Lagrangian particle-tracking

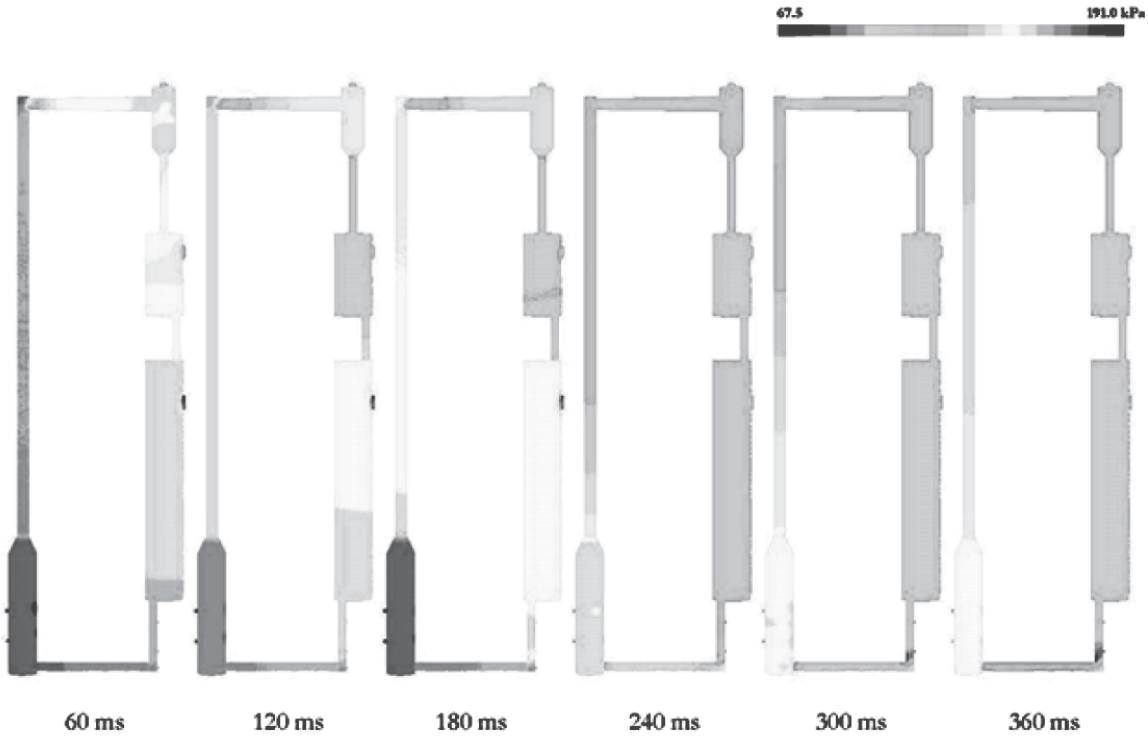

Figure 5(c): Pressure contours for cold flow inside the CLC apparatus

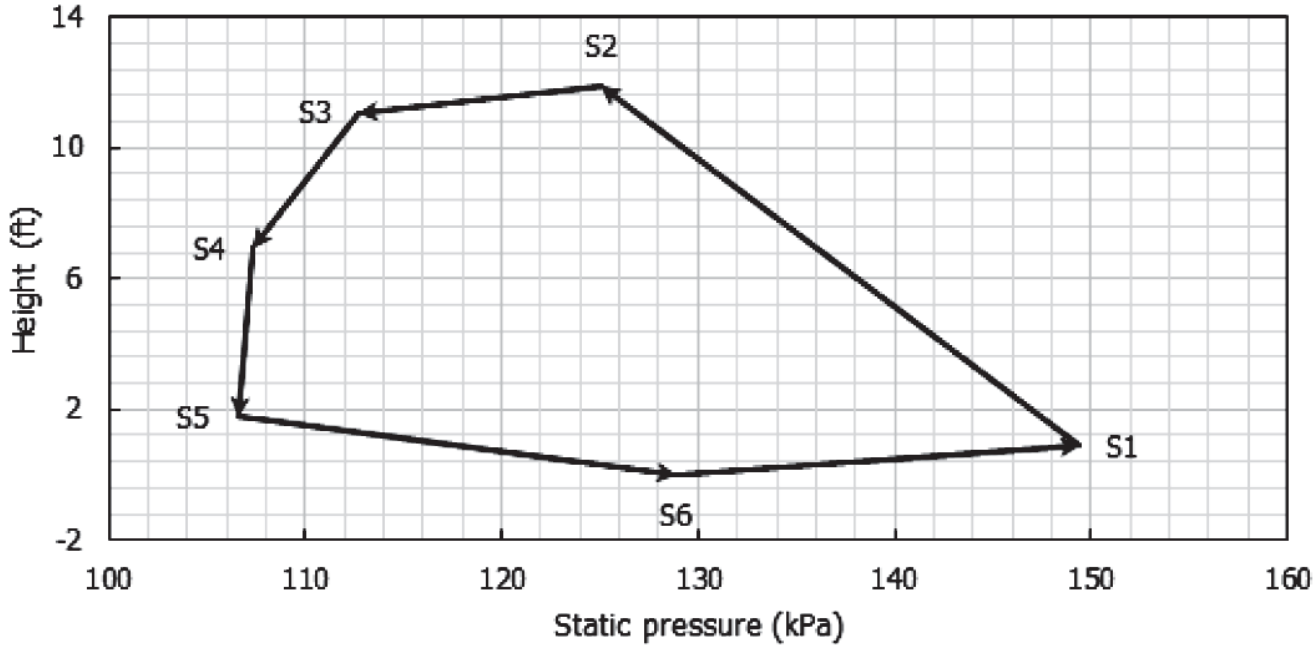

Figure 6: Static pressure at surfaces S1–S6 in the CD-CLC system shown in Figure 6 at t=360 ms

DEM approach employing the CLC reactor at NETL. The development of particle flow was investigated as well as the pressure contours. The static pressure contours and gradients showed evidence of favorable conditions for particle recirculation.

References

Abad, A., Mattisson, T., Lyngfelt, A., and Johansson, M., 2007, "The use of iron oxide as oxygen carrier in a chemical-looping reactor," Fuel, 86, pp. 1021-1035.

Andrus, H.E. et al, 2008, "Hybrid combustion-gasification chemical looping coal power technology development phase III-final report," National Energy Technology Laboratory, Albany, OR.

ANSYS, 2012a, "ANSYS FLUENT User's Guide," ANSYS, Inc., Canonsburg, PA.

ANSYS, 2012b, "ANSYS FLUENT Theory Guide," ANSYS, Inc., Canonsburg, PA.

Arrhenius, S., 1896, "On the influence of carbonic acid in the air upon the temperature of the ground," Philos. Mag., 41, pp. 237-277.

Banerjee, S. and Agarwal, R.K., 2015a, "Transient reacting flow simulation of spouted fluidized bed for coal-direct chemical looping combustion," J. Thermal Sci. Eng. Appl., 7(2). DOI: 10.1115/1.4029951.

Banerjee, S. and Agarwal, R.K., 2015b, "An Eulerian approach to CFD simulation of a chemical-looping combustion reactor with chemical reactions," Proc. 40th Int. Technical Conference on Clean Coal & Fuel Systems, Clearwater, FL.

Chong, Y.O., Nicklin, D.J., and Tait, P.J., 1986, "Solid exchange between adjacent fluid beds without gas mixing," Powder Technol. 47, pp. 151-156.

Deng, Z. et al., 2008, "Multiphase CFD modeling for a chemical looping combustion process (fuel reactor)," Chem. Eng. Tech., 31(12), pp. 1754-1766.

Ergun, S., 1952, "Fluid flow through packed columns," Chem. Eng. Prog., 48, pp. 89-94.

Fang, M. et al., 2003, "Experimental research on solid circulation in a twin fluidized bed system," Chem. Eng. J., 94, pp. 171-178.

Gidaspow, D., 1992, "Multiphase Flow and Fluidization," Academic Press, San Diego, CA.

Gryczka, O. et al., 2009, "Characterization and CFD modeling of the hydrodynamics of a prismatic spouted bed apparatus," Chem. Eng. Sci., 64, pp. 3352-3375.

Gunn, D.J., 1978, "Transfer of heat or mass to particles in fixed and fluidized beds," Int. J. Heat Mass Transfer, 21, pp. 467-476.

Hossain, M.M. and de Lasa, H.I., 2008, "Chemical-looping combustion (CLC) for inherent CO2 separations-a review," Chemical Engineering Science, 63, pp. 4433-4451.

IPCC, 2007, "Climate Change 2007: Synthesis Report. Contribution of Working Groups I, II and III to the Fourth Assessment Report of the Intergovernmental Panel on Climate Change [Core Writing Team, Pachauri, R.K., and Reisinger, A. (eds.)]," IPCC, Geneva, Switzerland.

Ishida, M., Jin, H., and Okamoto, T., 1996, "A fundamental study of a new kind of medium material for chemical-looping combustion," Energy & Fuels, 10(4), pp. 958-963.

Ishida, M., Zheng, D., and Akehata, T., 1987, "Evaluation of a chemical-looping-combustion power-generation system by graphic exergy analysis," Energy, 12(2), pp. 147-154.

Johansson, M., 2007, "Screening of oxygen-carrier particles based on iron-, man-ganese-, copper- and nickel oxides for use in chemical-looping technologies," Ph.D. dissertation, Chalmers University of Technology, Göteborg, Sweden.

Jung, J. and Gamwo, I., 2008, "Multiphase CFD-based models for chemical looping combustion process: fuel reactor modeling," Powder Technol., 183, pp. 401-409

Kruggel-Emden, H., Stepanek, F., and Munjiza, A., 2011, "A study on the role of reaction modeling in multi-phase CFD-based simulations of chemical looping combustion," Oil & Gas Sci. Tech., 66(2) pp. 313-331.

Link, J.M., 1975, "Development and validation of a discrete particle model of a spout-fluid bed granulator," Ph.D. dissertation, University of Twente, Enschede, The Netherlands.

Lun, C.K.K., Savage, S.B., Jeffrey, D.J., and Chepurniy, N., 1984, "Kinetic theories for granular flow: inelastic particles in Couette flow and slightly inelastic particles in general flow field." J. Fluid Mech., 140, pp. 223-256.

Lyngfelt, A., Leckner, B., and Mattisson, T., 2001, "A fluidized-bed combustion process with inherent CO2 separation; application of chemical-looping combustion," Chem. Eng. Sci., 56(10), pp. 3101-3113.

Mahalatkar, K., Kuhlman, J., Huckaby, E.D., and O'Brien, T., 2011a, "Computational fluid dynamic simulations of chemical looping fuel reactors utilizing gaseous fuels," Chem. Eng. Sci., 66(3), pp. 469-479.

Mahalatkar, K., Kuhlman, J., Huckaby, E.D., and O'Brien, T., 2011b, "CFD simulation of a chemical-looping fuel reactor utilizing solid fuel," Chem. Eng. Sci., 66(16), pp. 3617-3627.

Marion, J.L., 2006, "Technology options for controlling CO2 emissions from fossil fueled power plants," Proc. 5th Annual Conference on Carbon Capture and Sequestration, Alexandria, VA.

Mattisson, T. et al., 2005, "Capture of CO2 in Coal Combustion. ECSC Coal RTD Prog-ramme Final Report," ECSC-7220-PR125.

Parker, J., 2012, "Simulation of coal particles in a full chemical looping combustion system," CPFD Software, LLC, Albuquerque, NM.

Patankar, N.A. and Joseph, D.D., 2001, "Modeling and numerical simulation of particulate flows by the Eulerian-Lagrangian approach," Int. J. Multiphase Flow, 27, pp. 1659-1684.

Patil, D.J., Annaland, M.V., and Kuipers, J.A.M., 2004a, Critical comparison of hydro-dynamic models for gas-solid fluidized beds-Part I: Bubbling gas-solid fluidized beds operated with a jet, Chem. Eng. Sci., 60(1), pp. 57-72.

Patil, D.J., Annaland, M.V., and Kuipers, J.A.M., 2004b, Critical comparison of hydro-dynamic models for gas-solid fluidized beds-Part II: Freely bubbling gas-solid fluidized beds, Chem. Eng. Sci., 60(1), pp. 73-84.

Taylor, G.I., 1954, "The dispersion of matter in turbulent flow through pipes," Proc. R. Soc. London. Ser. A, Math. Phys. Sci., 223, pp. 446-448.

Wen, C.Y. and Yu, H.Y., 1966, "Mechanics of fluidization," Chem. Eng. Prog. Symp. Ser., 62, pp. 100-111.

Wolf, J., Anheden, M., and Yan, J., 2001, "Performance analysis of combined cycles with chemical looping combustion for CO2 capture," Proc. 18th International Pittsburgh Coal Conference, Pittsburgh, PA.